Biosensors and Bioelectronics 213 (2022) 114446

Contents lists available at ScienceDirect

Biosensors and Bioelectronics

journal homepage: www.elsevier.com/locate/bios

The Mn-modified porphyrin metal-organic framework with enhanced oxidase-like activity for sensitively colorimetric detection of glutathione

Xiang Lai [a], Yue Shen [a], Shoubei Gao [a], Yajing Chen [a], Yanshuai Cui [b,***], Dongxue Ning [c,**], Xianbing Ji [b], Zhiwei Liu [a], Longgang Wang [a,*]

[a] State Key Laboratory of Metastable Materials Science and Technology, Key Laboratory of Applied Chemistry, Nano-biotechnology Key Lab of Hebei Province, Yanshan University, Qinhuangdao, 066004, China
[b] Hebei University of Environmental Engineering, Qinhuangdao, 066102, China
[c] Qinhuangdao Huaheng Bioengineering Co., Ltd, Qinhuangdao, 066200, China

ARTICLE INFO

Keywords:
PCN-224
Oxidase-like activity
Glutathione
Colorimetry
Detection

ABSTRACT

The selective detection of glutathione (GSH) has been used as important colorimetric probe for human health. Herein, we used a facile method to synthesize manganese ions modified porphyrin metal-organic framework (PCN-224-Mn) with a size of 125.7 ± 14.2 nm and zeta potential of −3.9 ± 0.5 mV. We showed that PCN-224-Mn catalyzed oxidation of 3,3′,5,5′-tetramethylbenzidine (TMB) in the absence of H_2O_2, resulting in a blue-colored oxidized TMB (oxTMB) that exhibits oxidase-like activity. Furthermore, a simple colorimetric detection method for GSH was developed based on the oxidase-like activity of PCN-224-Mn. This method shows wide linear detection range of 0.5–60 μM for GSH with a much lower detection limit of 0.233 μM. Finally, the recovery of colorimetric sensor of PCN-224-Mn suggests its great potential as a biosensor. As the catalytically active site, the manganese porphyrin unit plays a major role in the oxidase-like property and detection ability of PCN-224-Mn. Our data suggest that GSH detection method using PCN-224-Mn has great potential in multiple applications in the future.

1. Introduction

Glutathione (GSH) is composed of cysteine, glutamic acid, and glycine, which exists in every cell of the body and plays a key role in many physiological processes. As an antioxidant, GSH is involved in the maintenance of maintain protein structure, intracellular signal transduction, gene transcription regulation, and immune response (Lee et al., 2018). The levels of GSH have been shown to be a key indicator to monitor diseases in skin, blood, cancer, and others (Chen et al., 2015; Yang et al., 2020). Therefore, quantitative detection of GSH is critical in the diagnosis of aforementioned diseases (Lin et al., 2022). Many GSH detection methods have been developed recently, including electrochemical, chromatography, fluorescence, colorimetry, and chemiluminescence methods (Huang et al., 2022; Li et al., 2017; Sun et al., 2022; Xie et al., 2021). In addition, chip-based microsensors have shown the potential for the construction of biosensors to monitor GSH levels (Peteu et al., 2021; Xu et al., 2019). Among these methods, colorimetry has attracted more and more attention because of its simplicity, low cost, and convenience (Liang et al., 2022).

In general, materials with peroxidase-like activity have been used for colorimetric detection of GSH (Chen et al., 2021a; Fan et al., 2021a; Yang et al., 2021). However, most of those protocols require H_2O_2 as a substrate to generate reactive oxygen species (ROS), such as hydroxyl radicals. Because H_2O_2 is easily decomposed by heat, it is necessary to develop oxidase-like enzymes whose activity does not depend on H_2O_2. The emergence of oxidase-like enzymes opens up a novel direction for development of biosensors. So far, materials based on precious metal nanomaterials with oxidase-like activity have attracted attention, including Cit-Pt NPs (Lin et al., 2021), Ru@V_2O_4 (Hou et al., 2021), and PVP-Pt NCs (Liu et al., 2021). However, the application of precious metal materials has been greatly restricted due to their high cost.

As a new class of functional material, metal-organic frameworks (MOFs) have numerous promising properties, such as energy storage (Gu et al., 2021), heterogeneous catalysis (Hao et al., 2021), and sensing

* Corresponding author.
** Corresponding author.
*** Corresponding author.
E-mail addresses: cuiyanshuai09@163.com (Y. Cui), 18346660455@163.com (D. Ning), lgwang@ysu.edu.cn (L. Wang).

https://doi.org/10.1016/j.bios.2022.114446
Received 7 March 2022; Received in revised form 22 May 2022; Accepted 30 May 2022
Available online 1 June 2022

(Fan et al., 2021b). In recent years, MOFs have also become promising enzyme mimetics (Huang et al., 2021). Compared with other artificial enzymes, MOF-mimic enzymes have more accessible catalytic sites and excellent properties that mimic enzyme catalytic activities. MOFs with an intrinsic enzyme-like activity have been developed recently, such as MIL-88 (Xu et al., 2021), ZIF-8 (Wang et al., 2020), Co-MOF (Wan et al., 2021), and Co/Mn-MOFs (Qi et al., 2019), providing possibilities for MOF-based colorimetric sensing applications in biological analysis. PCN-224 (porous coordination network-224) is a porphyrin Zr-MOF with simple and stable structure that is easy to be synthesized. The porphyrin cavity of PCN-224 provides an active site for some metals, resulting in a heme-like structure. When some metals are introduced into PCN-224, MOF materials with enzyme-like properties could be obtained, such as PCN-224-Pt (Zhang et al., 2018b), PdNPs@PCN-224 (Xia et al., 2021), and Fe@PCN-224 (Li et al., 2019). Therefore, metal-incorporated PCN-224 can provide a platform for the development and design of novel mimetic enzymes.

In this work, PCN-224 constructed by Zr_6 node and TCPP ligand was prepared. Then, Mn(II) was coordinated to the center of the porphyrin unit to produce Mn-modified MOFs, named as PCN-224-Mn. The manganese porphyrin unit in PCN-224-Mn served as an active site to mimic oxidase. The oxidase-like property was investigated by using TMB as the substrate. Based on this property, a colorimetric method was developed to detect GSH (Scheme S1). In addition, PCN-224-Mn was further employed in practical GSH detection in real sample. Therefore, as a MOF with oxidase-like activity, PCN-224-Mn shows promising applications in biochemical analyses.

2. Experimental section

We first constructed PCN-224 with Zr_6 node and TCPP ligand, and then incorporated Mn(II) into PCN-224 to form PCN-224-Mn. In order to explore the enzyme-like properties of PCN-224, many experiments were carried out such as oxidase-like activity of PCN-224-Mn, kinetic analysis, the mechanism of oxidase-like activity, colorimetric detection of GSH, and detection of GSH in real samples. The colorimetric method of GSH detection was established due to the enzyme-like properties of PCN-224-Mn and used in analysis of real samples.

2.1. Materials and apparatus

Zirconyl chloride octahydrate ($ZrClO_2{\cdot}8H_2O$), benzoic acid (BA), 3,3′,5,5′-tetramethylbenzidine (TMB), o-phenylenediamine (OPD), 2,2′-azino-bis (3-ethylbenzothiazoline-6-sulfonic acid) (ABTS), p-benzoquinone (BQ), ethylenediaminetetraacetic acid disodium salt (EDTA-2Na), sodium azide (NaN_3), glutathione (GSH), HAc, and NaAc were purchased from Aladdin (Shanghai, China). Manganese chloride tetrahydrate ($MnCl_2{\cdot}4H_2O$) was purchased from Shanghai Yien Chemical Technology Co., Ltd (Shanghai, China). *N,N*-dimethylformamide (DMF) and isopropanol (IPA) were purchased from Kemio Chemical Reagent Co., Ltd (Tianjin, China). Tetrakis(4-carboxyphenyl) porphyrin (TCPP) as purchased from Bide Pharmatech Ltd (Shanghai, China). Human blood was taken from healthy volunteers. Food-grade glutathione was purchased from Liyuan Biotechnology Co., Ltd.

The transmission electron microscopy (TEM) and energy dispersive spectroscopy (EDS) analysis were performed on HT 7700. The scanning electron microscope (SEM) images were collected on SUPRA 55. The hydrodynamic size and zeta potential were measured by Zetasizer Nano-ZS90 based on dynamic light scattering (DLS) technology. UV-vis spectra were recorded on a UV-TU1810PC spectrophotometer. The Fluorescence (FL) spectra were recorded on F-7000. The infrared (IR) spectra were recorded on Nicolet iS10. The X-ray photoelectron spectroscopy (XPS) spectra were performed on Thermo Scientific EACALAB Xi+. The inductively coupled plasma-atomic emission spectrometry (ICP-AES) was performed on iCAP 6300 Radial. The X-ray diffraction (XRD) data were measured with a Rigaku D/max-2550 diffractometer. The thermogravimetric analysis (TGA) data was determined by STA 409 PC thermogravimetric analyzer. An MSC-100 Thermo Shaker was used for incubation.

2.2. The synthesis of PCN-224-Mn

The synthesis of PCN-224 was reported previously (Park et al., 2016). Typically, $ZrOCl_8{\cdot}H_2O$ (180 mg), TCPP (60 mg), and BA (1.68 g) were dissolved in 60 mL DMF, and then the mixture was incubated in a water bath at 90 °C for 5 h. The PCN-224 particles were separated by centrifugation (9000 rpm, 20 min). The obtained purple solid particles were washed for 3 times with DMF and ultrapure water. Subsequently, $MnCl_2{\cdot}4H_2O$ (100 mg) and obtained PCN-224 (50 mg) were dissolved in 20 mL DMF by stirring for 12 h at 120 °C in an oil bath. PCN-224-Mn was collected by centrifugation and dried in a vacuum oven.

2.3. Oxidase-like activity of PCN-224-Mn

The oxidase-like activity of PCN-224-Mn was monitored by oxidizing TMB. In brief, 50 μL of PCN-224-Mn (1 mg/mL), 1000 μL of TMB (0.8 mM) and 400 μL of HAc-NaAc buffer (pH 4.0, 0.2 M) were mixed and incubated at 25 °C for 5 min. The absorption spectrum was obtained by recording in the range of 300–800 nm. In addition, two other substrates (OPD and ABTS), were used to assess oxidase-like activity using the same method. The relative activity of PCN-224-Mn was evaluated under different experimental conditions, including pH value from 2.0 to 11.0, and temperature from 15 to 70 °C.

2.4. Kinetic analysis

The kinetic analysis was conducted in HAc-NaAc buffer (pH 4.0, 0.2 M) containing various concentrations of TMB (0.055–0.50 mM). We added 50 μL of PCN-224-Mn (1 mg/mL) to the above solutions to the total volume of 1450 μL. The absorbance at various concentrations of TMB were recorded at 652 nm using time scanning mode. The K_m and V_{max} values of PCN-224-Mn oxidized TMB were calculated using Michaelis-Menten equation and Lineweaver-Burk plot (Dong et al., 2021):

$$\frac{1}{v}=\frac{K_m}{V_{max}}\times\frac{1}{[S]}+\frac{1}{V_{max}} \quad (1)$$

where v and V_{max} stand for the initial and the maximum initial reaction rate, respectively. [S] and K_m stand for the substrate concentration and Michaelis constant, respectively.

2.5. The mechanism of oxidase-like activity

First, the effect of dissolved oxygen in the reaction solution was analyzed. 1 mL of PCN-224-Mn (1 mg/mL) and 5 mL of TMB (0.8 mM) were bubbled with N_2 for 30 min to remove oxygen. 50 μL PCN-224-Mn (1 mg/mL) and 1000 μL TMB (0.8 mM) were mixed and incubated at 25 °C for 5 min, then the absorption spectrum was recorded.

Secondly, the nature of ROS generated during the experiments was investigated by the effects of different free radical scavengers on the oxidase-like activity. These free radical scavengers include NaN_3, IPA, BQ, and EDTA-2Na. To the reaction solution of 50 μL PCN-224-Mn (1 mg/mL), 1000 μL TMB (0.8 mM), 300 μL NaAc-HAc (pH = 4, 0.2 M), add 100 μL of different capture agents at different concentrations were added. The absorbance was measured after incubation at 25 °C for 5 min. The concentrations of these free radical scavengers were 1 mM, 5 mM, and 10 mM, respectively.

2.6. Colorimetric detection of GSH

For the detection of GSH, 50 μL PCN-224-Mn (1 mg/mL), 1000 μL

TMB (0.8 mM), and 200 μL HAc-NaAc buffer (pH 4.0, 0.2 M) were mixed and incubated at 25 °C for 5 min. Then, different concentrations of GSH were added for further incubation for 5 min. The color of the reaction solution was observed and the absorbance of each reaction solution at the wavelength of 500–800 nm was recorded.

In addition to GSH, other interfering substances were also used for the interference experiment. These interfering substances include amino acids (phenylalanine, tyrosine, glycine, alanine, lysine, proline, leucine, histidine), inorganic ions (K^+, Na^+, Ca^{2+}, Mg^{2+}), and sugars (maltose, lactose, fructose, glucose). The concentrations of these substance used was 1200 μM.

2.7. Detection of GSH in real samples

To illustrate application of PCN-224-Mn in GSH detection, human serum and food grade glutathione were used. Human blood was taken from healthy volunteers, and the supernatant was obtained after centrifugation at 5000 rpm for 3 min. The supernatant was diluted 5 times with ultrapure water. Then, 200 μL of diluted serum was added to the system [TMB + PCN-224-Mn], and the GSH concentration was detected using the above-mentioned colorimetric method. Food-grade glutathione was also analyzed by a similar method.

3. Results and discussion

Zr_6 node and TCPP ligand were used to construct PCN-224, which was incorporated Mn(II) to form PCN-224-Mn. The structure of PCN-224-Mn was characterized by TEM, XPS and DLS. Then, PCN-224-Mn had oxidase-like activity, and its activity was related to the superoxide anions produced in the system. A colorimetric method for the detection was established base on the oxidase-like activity of PCN-224-Mn. The concentration of GSH in real samples was measured using this method.

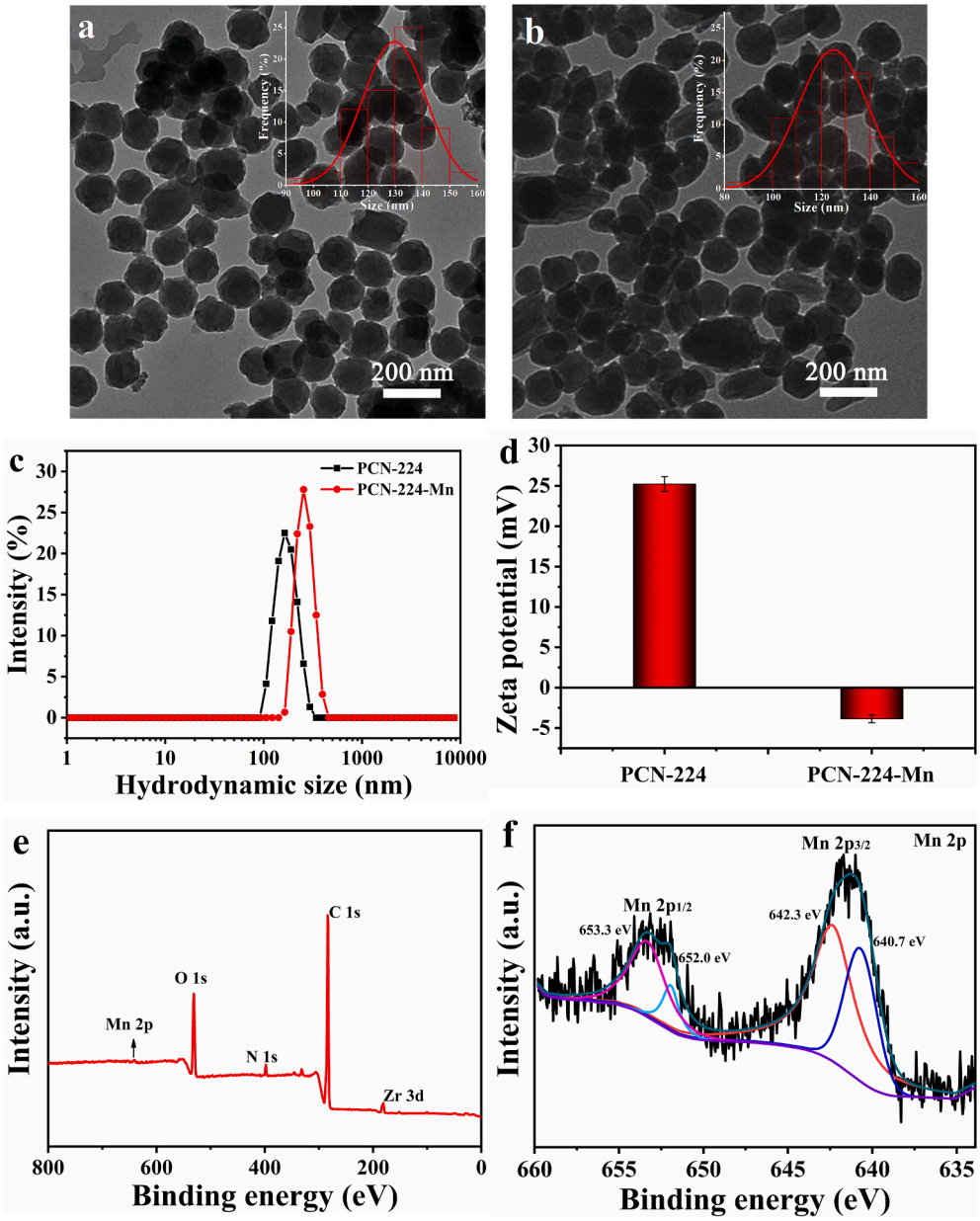

Fig. 1. TEM images of (a) PCN-224 and (b) PCN-224-Mn. (c) The hydrodynamic size and (d) zeta potential of PCN-224 and PCN-224-Mn; XPS spectra of PCN-224-Mn: (e) survey spectra, (f) high resolution XPS spectra of Mn 2p.

3.1. Characterization of PCN-224-Mn

PCN-224 is a stable metal-organic framework consisting of Zr_6 node and TCPP ligand. In this work, Mn(II) was inserted into PCN-224 by passing through an oil bath of 120 °C to generate PCN-224-Mn. The features of PCN-224 and PCN-224-Mn were monitored by TEM and SEM imaging as shown in Fig. 1 and Fig. S1. PCN-224 was successfully synthesized with spherical structure and uniform size. The morphology of PCN-224-Mn is similar to PCN-224. After statistical analysis, the sizes of PCN-224 and PCN-224-Mn were 129.7 ± 11.6 nm and 125.7 ± 14.2 nm, respectively. The state of particles in solution was measured by DLS (He et al., 2022). PCN-224 showed a hydrodynamic size of 140 nm, while the size of PCN-224-Mn was 180 nm (Fig. 1c). The hydrodynamic size of PCN-224-Mn was larger than that of PCN-224. The formation of larger hydrodynamic size of PCN-224-Mn observed by DLS may be attributed to enhanced hydration of PCN-224-Mn (Li et al., 2019). Moreover, the zeta potential of PCN-224 and PCN-224-Mn was 25.2 ± 0.9 mV and −3.9 ± 0.5 mV, respectively (Fig. 1d).

The elemental composition of PCN-224-Mn was analyzed by XPS, and the spectrum of PCN-224-Mn is shown in Fig. 1e. These peaks represent C, N, O, Zr and Mn elements, which is consistent with the EDS results. The high-resolution of Mn 2p exhibited two peaks at 653.3 eV and 641.5 eV, which are likely Mn $2p_{1/2}$ and Mn $2p_{3/2}$ (Fig. 1f). The peak of Mn $2p_{3/2}$ could be deconvoluted into two peaks at 642.3 eV and 640.7 eV, which belong to Mn^{3+} and Mn^{2+}, respectively. In addition, the asymmetry of the Mn $2p_{3/2}$ peak indicates the existence of mixed-valence manganese (Qi et al., 2019). The Mn content measured by ICP-AES is 4.34 wt%.

The spectral difference among TCPP, PCN-224, and PCN-224-Mn was shown in Fig. 2 and Fig. S3. PCN-224 exhibited a strong peak at 425 nm and four weak peaks between 500 and 700 nm. These absorption peaks were likely attributed to the Soret band and Q-bands of TCPP ligand, respectively (Tao et al., 2021). Compared with PCN-224, the UV-vis absorption of PCN-224-Mn presented a great change and the Q-bands of PCN-224-Mn disappeared, indicating that the porphyrin ring was coordinated with Mn(II). Moreover, FTIR spectroscopy was used to analyze the structure of PCN-224-Mn. The asymmetric vibrational intensity of C–OH (1246 cm^{-1}) and C═O (1696 cm^{-1}) of PCN-224 and PCN-224-Mn was much lower than that of TCPP, which was attributed to the coordination between Zr_6 cluster and carboxyl groups (Fig. 2b). The disappearance of N–H bond (3310 cm^{-1} and 965 cm^{-1}) and the formation of N–Mn bond (1010 cm^{-1}) were observed in PCN-224-Mn (Fig. 2c). Remarkably, compared with PCN-224, PCN-224-Mn exhibited fluorescence quenching when excited at 425 nm (Fig. S2). The coordination of Mn(II) with the nitrogen atoms in the porphyrin structure quenched the fluorescence of PCN-224-Mn (Zhang et al., 2018a). As shown in Fig. 2d, EDS elemental analysis confirmed that C, N, O, Zr and Mn were uniformly distributed in PCN-224-Mn, Cu likely came from the test copper mesh. These results indicate the coordination of the porphyrin ring with Mn, and the successful preparation of PCN-224-Mn.

As shown in Fig. S3, XRD results revealed that PCN-224 had a good phase purity of consistency with the simulated PCN-224 structure. However, the crystallinity of PCN-224-Mn became poorer compared with PCN-224. The TGA curves of PCN-224 and PCN-224-Mn were shown in Fig. S5, which indicated the same weightlessness characteristics. The weight loss of the two structures after treated with high temperature (500 °C) may be attributed to the dehydration of the Zr_6 node (Ji et al., 2020; Lin et al., 2019). The weight loss above 500 °C can be attributed to the decomposition of the porphyrin ligand (Ji et al., 2020). Moreover, the total weight loss of PCN-224 and PCN-224-Mn was about 46% and 38%, respectively.

3.2. Oxidase-like activity of PCN-224-Mn

Some substrates with special optical phenomena are used to build sensors (Xu K. 2021). To test whether PCN-224-Mn as well as TCPP ligand and PCN-224 show oxidase-like activity, the absorbance of four groups was measured from 300 to 800 nm. As shown in Fig. 3a, TCPP

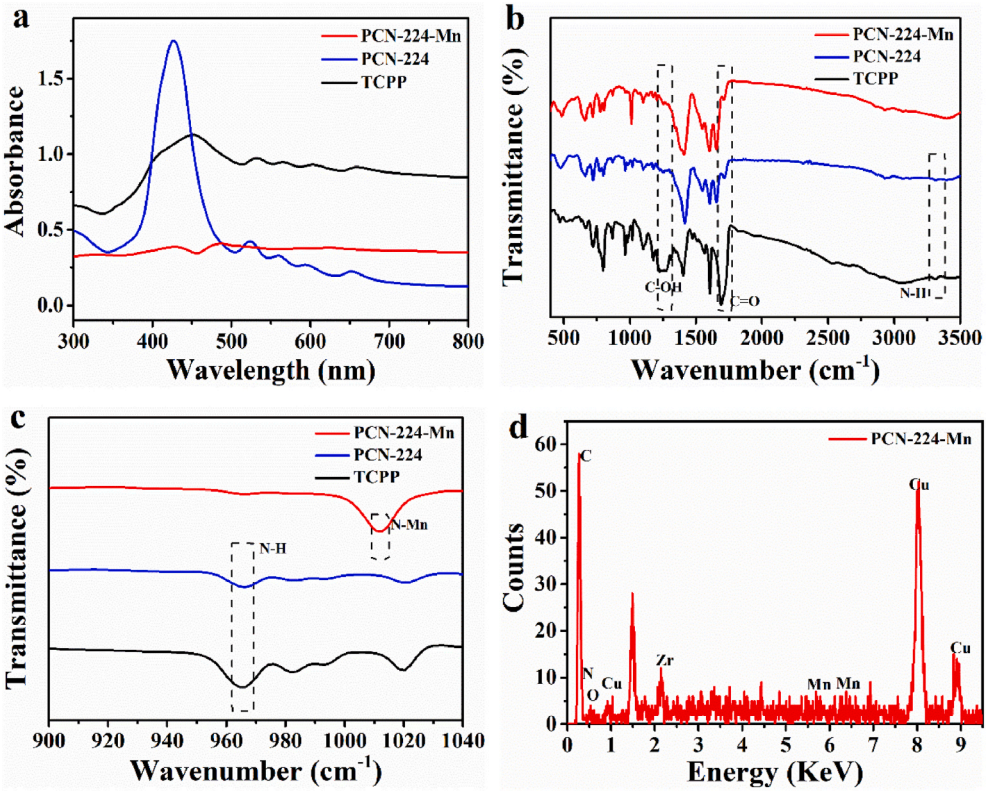

Fig. 2. (a) UV-vis spectra, (b) FTIR spectra and (c) magnified FTIR spectra of TCPP, PCN-224 and PCN-224-Mn, (d) EDS spectrum of PCN-224-Mn.

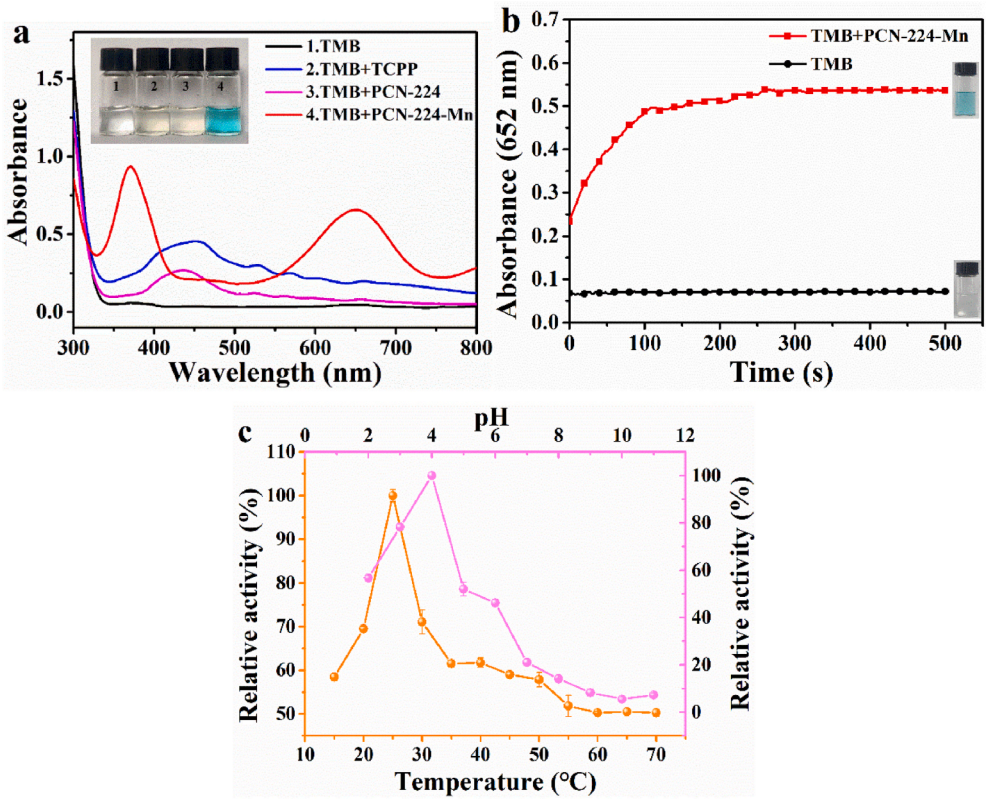

Fig. 3. (a) UV-vis spectra of each system and (b) time-dependent absorbance changes at 652 nm in TMB and TMB + PCN-224-Mn. (c) The oxidase-like activity of PCN-224-Mn depends on pH and temperature.

and PCN-224 did not react with TMB, but PCN-224-Mn catalyzed oxidation of TMB to produce oxTMB and cause color change to blue, indicating the oxidase-like activity of PCN-224-Mn. To further verify this, the change of absorbance of PCN-224-Mn within 500 s was followed (Fig. 3b). Strikingly, the absorbance of [TMB + PCN-224-Mn] group increased sharply to 0.5 within 100 s, and the color of solution rapidly changed to blue. For the oxidase-like catalysis of PCN-224-Mn, the absorbance reached saturation after some time, which meant TMB in the reaction system was completely converted to oxTMB. Under the same conditions, the absorbance and solution color of [TMB] group remained almost unchanged. In addition, typical substrates such as OPD and ABTS were also used to evaluate the oxidase-like activity of PCN-224-Mn (Fig. S5a). After PCN-224-Mn was added into the solution containing these substrates, color changes occurred. Consistently, PCN-224-Mn reacted with OPD and ABTS to generate oxOPD and oxABTS with maximum absorption peaks at 450 and 420 nm, respectively (Fig. S5b).

Similar to many enzyme mimics, we speculated that the catalytic activity of PCN-224-Mn also depends on pH and temperature. Therefore, the catalytic activity of PCN-224-Mn was compared under the conditions of pH from 2.0 to 11.0 or temperature from 15 to 70 °C. As displayed in Fig. 3c, the catalytic activity of PCN-224-Mn gradually increased as pH changed from 2 to 4, and gradually decreased as pH changed from 4 to 11. Hence, PCN-224-Mn exhibits the maximum activity at pH 4.0, indicating that TMB was easily oxidized in a weak acidic condition. This might be related to the status of PCN-224-Mn. In addition, we examined temperature-dependent catalytic activity of PCN-224-Mn at pH 4.0 from 15 to 70 °C (Fig. 3c). The optimal temperature for PCN-224-Mn as an artificial enzyme was 25 °C. Therefore, the optimal conditions for studying the oxidase activity of PCN-224-Mn on the substrate TMB are pH 4.0 and temperature 25 °C.

3.3. Steady-state kinetic

We further tested the steady-state kinetics of the substrate on the [TMB + PCN-224-Mn] group to obtain more details about the properties of the oxidase-like activity. The typical Michaelis-Menten curve was obtained by plotting the corresponding initial reaction rate and substrate concentration (Fig. 4a). By taking the double reciprocal of the data in Fig. 4a, the Lineweaver-Burk diagram (Fig. 4b) was obtained. The parameters (K_m and V_{max}) were calculated, and compared with other catalysts. The K_m was calculated to be 0.243 mM, which was lower than those of catalysts in Table S1. This result suggests that PCN-224-Mn had a decent affinity toward TMB. The excellent affinity of PCN-224-Mn for TMB is likely attributed to its own negative charge. Since the amine group of TMB is positively charged, and negatively charged mimetic enzymes can exhibit stronger affinity for TMB (Chen et al., 2021b).

3.4. Mechanistic studies

The possible mechanism of the oxidase-like activity of PCN-224-Mn is derived from the conversion of dissolved oxygen into ROS during the reaction. As shown in Fig. 5a, the absorbance at 652 nm was found to be greatly reduced in the N_2 purged solution. The absorbance of [TMB + PCN-224-Mn] at 652 nm after N_2 gas treatment was 0.43 times of the value obtained in air. In the [TMB + PCN-224-Mn] group, the oxidation reaction depends on the reactive ROS generated by dissolved oxygen. To explore the effect of ROS on this reaction, NaN_3, IPA, BQ and EDTA-2Na were used as scavengers to singlet oxygen ($^1O_2$), hydroxyl radicals (•OH), superoxide anions ($O_2^{\bullet-}$) and hole (h^+), respectively. As shown in Fig. 5b, compared with the control experiment, the catalytic activity was significantly reduced in the presence of BQ, while other scavengers only showed weak effect on the reaction. The results suggest that $O_2^{\bullet-}$ is produced in the [TMB + PCN-224-Mn] system. Thus, PCN-224-Mn likely catalyzes the conversion of dissolved oxygen to $O_2^{\bullet-}$ radicals, which

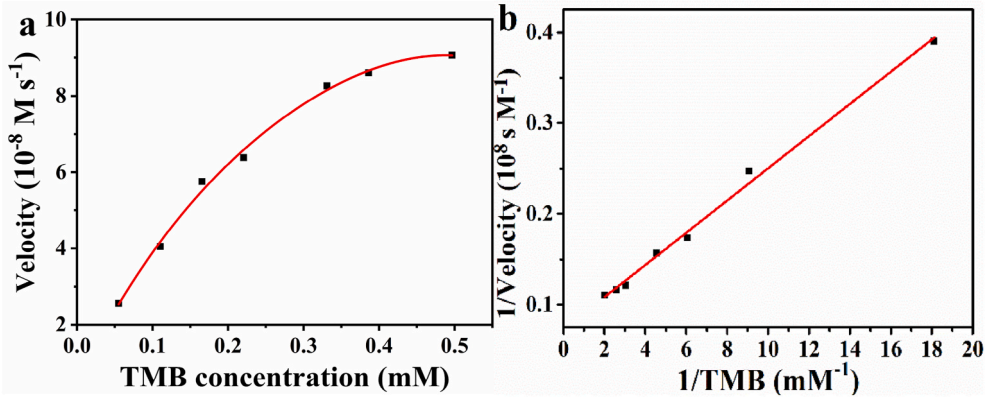

Fig. 4. (a) Michaelis-Menten curve of the PCN-224-Mn under different TMB concentrations; (b) corresponding Lineweaver-Burk diagram.

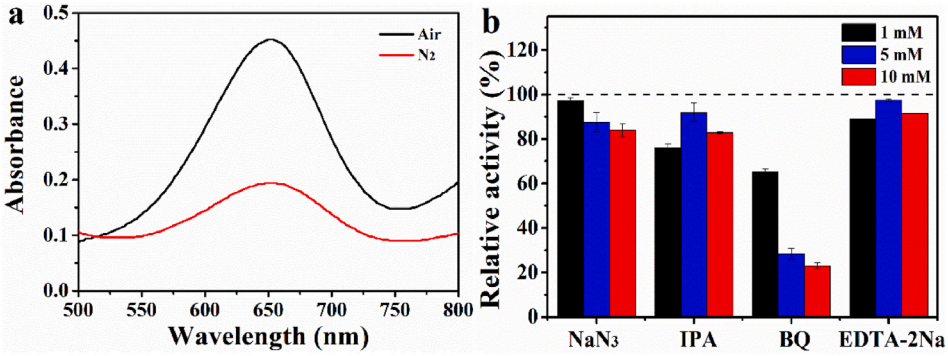

Fig. 5. (a) The UV-vis spectra of [TMB + PCN-224-Mn] system in air or N_2, (b) inhibition of different scavenger for [TMB + PCN-224-Mn] system.

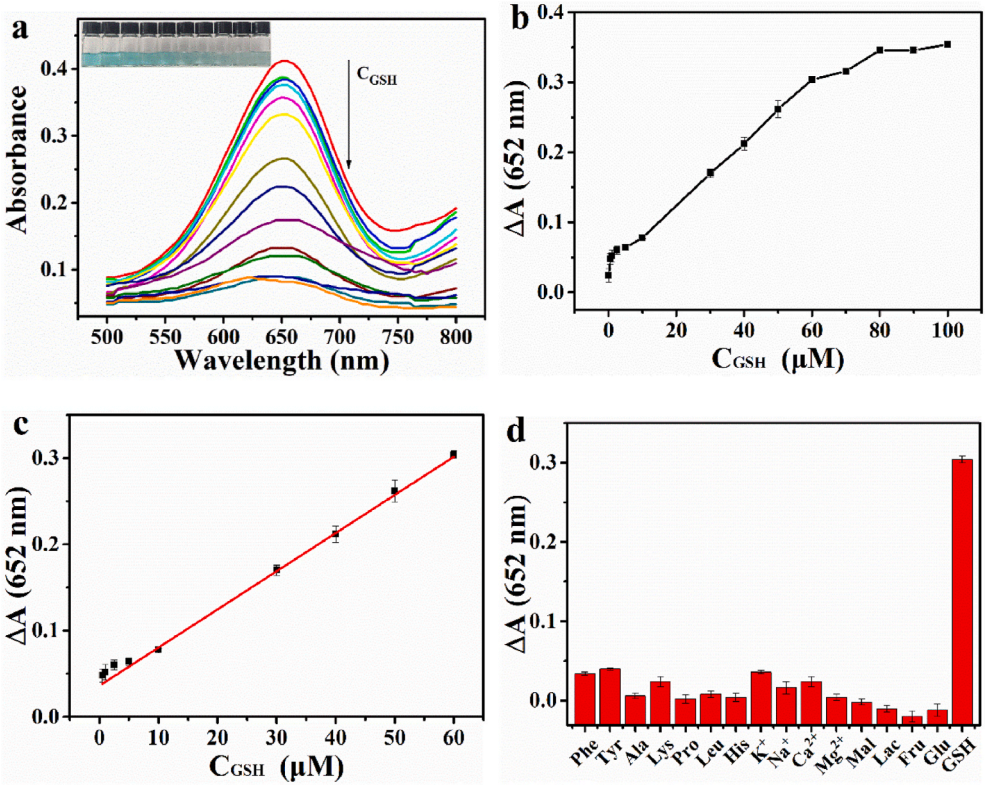

Fig. 6. (a) UV-vis absorption curves and (b) absorbance at 652 nm of [TMB + PCN-224-Mn] with various concentration of GSH; (c) linear calibration chart of GSH detection, (d) the absorbance of GSH (60 μM) and other interfering substances (1200 μM).

further oxidize TMB into blue oxTMB.

3.5. GSH detection

GSH presents naturally in the plasma of human body. There is an intimate relationship between glutathione metabolism and diseases such as cancer, cardiovascular and ophthalmic diseases (Lee et al., 2018). Therefore, it is important to exploit a fast and reliable method to detect GSH in human samples. Because of the antioxidant properties, GSH has the ability of reducing oxTMB to TMB, showing obvious color change. Therefore, a simple GSH detection method was established by combing this property of GSH with the oxidase-like activity of PCN-224-Mn.

As shown in Fig. 6a, when different concentrations of GSH were added to the [TMB + PCN-224-Mn] group, a gradual decrease in absorbance at 652 nm was observed with increasing GSH concentration. Fig. 6b showed that the absorbance change of oxTMB at 652 nm (ΔA) was directly proportional to GSH concentration. In Fig. 6c, the ΔA displayed a linear relationship with GSH concentration, expressed as $\Delta A = 0.0043C_{[GSH]}+0.03612$ ($R^2 = 0.995$). This linear trend was further presented in Fig. S6. Moreover, the linear range of GSH concentration was from 0.5 to 60 μM, and the detection limit was 0.233 μM. Other reported materials with oxidase-like property for colorimetric detection of GSH sensors were summarized in Table S2, and the method based on PCN-224-Mn showed a wider linear range and lower detection limit.

To analyze the specificity of PCN-224-Mn-based method, several amino acids, inorganic ions, and various sugar were set as controls. In this experiment, the concentration of the substances listed above was 1200 μM, while GSH concentration was 60 μM. Only GSH obviously inhibited the color reaction of TMB (Fig. 6d), indicating that this assay shows an excellent selectivity for GSH detection.

In order to further verify the reliability and accuracy of established method, human plasma and food-grade GSH were measured, and standard addition method was used to carry out recovery experiments. As shown in Table S3, the acceptable recovery rate was from 101.51% to 110.97%, and the relative standard deviation (RSD) was less than 6%. Thus, the established method showed satisfactory results for GSH detection in these samples. These results indicate that this [TMB + PCN-224-Mn]-based colorimetric method is reliable for GSH detection.

4. Conclusions

In summary, PCN-224-Mn with oxidase-like activity was successfully synthesized by simple coordination. The mechanism of the catalytic reaction was analyzed, and the enzyme activity of PCN-224-Mn came from $O_2^{\bullet-}$. The oxidase-like catalytic activity of PCN-224-Mn was affected by pH and temperature. Based on the oxidase-like property of PCN-224-Mn, a simple and sensitive colorimetric method for GSH detection was developed, which presented a linear response to GSH concentration ranging from 0.5 to 60 μM with the detection limit of 0.233 μM. The human serum samples and food-grade GSH were measured for GSH concentration using this method with decent recovery. Therefore, in this work we successfully developed a colorimetric sensing method using porphyrin MOFs, and our results suggest potential applications of this method in catalysis, medical analysis, and biosensor.

CRediT authorship contribution statement

Xiang Lai: Investigation, Writing – original draft. **Yue Shen:** Investigation. **Shoubei Gao:** Visualization. **Yajing Chen:** Investigation. **Yanshuai Cui:** Methodology, Writing – review & editing. **Dongxue Ning:** Conceptualization, Writing – review & editing. **Xianbing Ji:** Writing – review & editing. **Zhiwei Liu:** Methodology. **Longgang Wang:** Supervision, Writing – review & editing.

Declaration of competing interest

The authors declare that they have no known competing financial interests or personal relationships that could have appeared to influence the work reported in this paper.

Acknowledgments

This research was funded by Natural Science Foundation of Hebei Province (B2017203229), Youth Foundation Project supported by the Hebei Education Department of China (QN2022124), Key Program of Hebei University of Environmental Engineering (2020ZRZD02), Talent Training Programs of Hebei Province (A201901068, A201901069), Scientific Research Key Projects of Education Department of Hebei Province (ZD2019024) and Science and Technology Support Program of Qinhuangdao (202101A007). We would like to thank the shiyanjia lab (www.shiyanjia.com) for the XPS test.

Appendix A. Supplementary data

Supplementary data to this article can be found online at https://doi.org/10.1016/j.bios.2022.114446.

References

Chen, C., Liu, W., Xu, C., Liu, W., 2015. Biosens. Bioelectron. 71, 68–74.
Chen, L., Li, X., Li, Z., Liu, K., Xie, J., 2021. RSC Adv. 12 (1), 595–601.
Chen, T., Cao, J., Bao, X., Peng, Y., Liu, L., Fu, W., 2021. RSC Adv. 11 (63), 39966–39977.
Dong, L., Li, R., Wang, L., Lan, X., Sun, H., Zhao, Y., Wang, L., 2021. Int. J. Biol. Macromol. 172, 289–298.
Fan, L., Ji, X., Lin, G., Liu, K., Chen, S., Ma, G., Xue, W., Zhang, X., Wang, L., 2021. Microchem. J. 166.
Fan, M.Y., Yu, H.H., Fu, P., Su, Z.M., Li, X., Hu, X.L., Gao, F.W., Pan, Q.Q., 2021. Dyes Pigments 185, 108834.
Gu, Y., Miao, L., Yin, Y., Liu, M., Gan, L., Li, L., 2021. Chin. Chem. Lett. 32 (4), 1491–1496.
Hao, M., Qiu, M., Yang, H., Hu, B., Wang, X., 2021. Sci. Total Environ. 760, 143333.
He, J., Wang, J., Gao, S., Cui, Y., Ji, X., Zhang, X., Wang, L., 2022. Int. J. Pharm. 615, 121489, 121489.
Hou, J.J., Jia, P., Yang, K.R., Bu, T., Sun, X.Y., Wang, L., 2021. Sensor. Actuat. B chem. 344, 10.
Huang, X., Zhang, S., Tang, Y., Zhang, X., Bai, Y., Pang, H., 2021. Coord. Chem. Rev. 449, 214216.
Huang, Z., Yu, S., Jian, M., Weng, Z., Deng, H., Peng, H., Chen, W., 2022. Anal. Chem. 94 (4), 2341–2347.
Ji, J., Liu, F., Yang, W., Tan, M., Luo, W., Yin, S.F., 2020. ChemCatChem 12 (17), 4331–4338.
Lee, S., Li, J., Xin, Z., Yin, J., Yoon, J., 2018. Coord. Chem. Rev. 366, 29–68.
Li, T., Hu, P., Li, J., Huang, P., Tong, W., Gao, C., 2019. Colloids Surf., A 577, 456–463.
Li, Y., Liu, W.M., Zhang, P.P., Zhang, H.Y., Wu, J.S., Ge, J.C., Wang, P.F., 2017. Biosens. Bioelectron. 90, 117–124.
Liang, Y., Li, H., Fan, L., Li, R., Cui, Y., Ji, X., Xiao, H., Hu, J., Wang, L., 2022. Colloids Surf., A 633, 127797.
Lin, G., Si, M., Wang, L., Wei, S., Lu, W., Liu, H., Zhang, Y., Li, D., Chen, T., 2022. Adv. Opt. Mater., 2102306
Lin, W., Gong, J., Fang, L., Jiang, K., 2019. Z. Anorg. Allg. Chem. 645 (18–19), 1161–1164.
Lin, X., Zhu, Z., Lin, D., Bao, Q., Gao, Y., Liu, Q., Liu, A., Lin, L., Lin, X., 2021. Talanta 234, 122647.
Liu, X.L., Tian, M.M., Li, C.Y., Tian, F.S., 2021. Colloids Surf., A 625, 126985.
Park, J., Jiang, Q., Feng, D., Mao, L., Zhou, H.C., 2016. J. Am. Chem. Soc. 138 (10), 3518–3525.
Peteu, S.F., Russell, S.A., Galligan, J.J., Swain, G.M., 2021. Electroanalysis 33 (2), 495–505.
Qi, X., Tian, H., Dang, X., Fan, Y., Zhang, Y., Zhao, H., 2019. Anal. Methods 11 (8), 1111–1124.
Sun, X.Y., Wang, C., Li, P., Shao, Z.Y., Xia, J., Liu, Q., Shen, F., Fang, Y., 2022. Food Chem. 372, 131142.
Tao, Y., Sun, Y., Shi, K., Pei, P., Ge, F., Yang, K., Liu, T., 2021. Biomater. Sci. 9 (8), 2947–2954.
Wan, H., Wang, Y., Chen, J., Meng, H.M., Li, Z., 2021. Microchim. Acta 188 (4).
Wang, Y., Liu, X., Wang, M., Wang, X., Li, J., 2020. Sensor. Actuat. B chem. 329, 129115.
Xia, M., Mao, C., Guo, Y., Pu, L., Zhang, Y., 2021. Colloids Interface Sci. Commun. 41, 100382.
Xie, J., Cheng, D., Li, P., Xu, Z., Zhu, X., Zhang, Y., Li, H., Liu, X., Liu, M., Yao, S., 2021. ACS Appl. Nano Mater. 4 (5), 4853–4862.

Xu, K., Chen, Y., Okhai, T.A., Snyman, L.W., 2019. Opt. Mater. Express 9 (10), 3985–3997.
Xu, K., 2021. J. Micromech. Microeng. 31 (5), 054001.
Xu, Z., Long, L.-l., Chen, Y.-q., Chen, M.-L., Cheng, Y.-H., 2021. Food Chem. 338, 128039.
Yang, W., Weng, C.Y., Li, X.Y., He, H.L., Fei, J.W., Xu, W., Yan, X.Q., Zhu, W.Y., Zhang, H.S., Zhou, X.M., 2021. Sensor. Actuat. B chem. 338, 129844.
Yang, X.J., Li, R.S., Li, C.M., Li, Y.F., Huang, C.Z., 2020. Talanta 215, 120928.
Zhang, W., Lu, J., Gao, X., Li, P., Zhang, W., Ma, Y., Wang, H., Tang, B., 2018. Angew. Chem. Int. Ed. 57 (18), 4891–4896.
Zhang, Y., Wang, F., Liu, C., Wang, Z., Kang, L., Huang, Y., Dong, K., Ren, J., Qu, X., 2018. ACS Nano 12 (1), 651–661.